

Digital Processing of the Mariner 6 and 7 Pictures

T. C. RINDFLEISCH, J. A. DUNNE, H. J. FRIEDEN,
W. D. STROMBERG, AND R. M. RUIZ

*Space Sciences Division, Jet Propulsion Laboratory
Pasadena, California 91103*

The Mariner Mars 1969 television camera system was a vidicon-based digital system and included a complex on-board video encoding and recording scheme. The spacecraft video processing was designed to maximize the volume of data returned and the encoded discriminability of the low-contrast surface detail of Mars. The ground-based photometric reconstruction of the Mariner photographs, as well as the correction of inherent vidicon camera distortion effects necessary to achieve television experiment objectives, required use of a digital computer to process the pictures. The digital techniques developed to reconstruct the spacecraft encoder effects and to correct for camera distortions are described and examples shown of the processed results. Specific distortion corrections that are considered include the removal of structured system noises, the removal of sensor residual image, the correction of photometric sensitivity nonuniformities and nonlinearities, the correction of geometric distortions, and the correction of modulation transfer limitations.

As all physically realizable instruments influence the data they collect, the Mariner Mars 1969 television cameras left their signatures on the imagery they returned to earth. Analyses of the Mariner photographs must be performed with the knowledge that Mars was observed through the spacecraft cameras, and any distortions introduced by the camera system processes potentially affect the results. This is particularly important for the Mariner 1969 photographs because of the complex video system design that was chosen to optimally record the low-contrast features of Mars and to maximize the quantity of data returned by the two flyby missions.

For some photointerpretive uses of the data, all that is required is a qualitative understanding of the camera-system properties and an optimum contrast display of the data after noise removal, geometric rectification, and edge enhancement as discussed in the paper by Dunne *et al* [1971]. The careful measurement of scene luminance and geometric properties and even the most careful and intensive photointerpretive evaluations of the pictures, however, require the precise calibration and removal of camera-system effects. The purpose of this paper is to describe the digital-computer techniques used to quantify and correct for the systematic video-data distortions, so that subsequent measurements

and interpretations of the imagery can be based on information as representative of the Martian surface as possible.

The succeeding sections will describe, from the point of view of image processing, the performance characteristics of the vidicon cameras and data-encoding electronics on board the spacecraft, the over-all flow of the various Mariner 1969 video-data streams through the rectification processing, and the approaches used for the correction of the data distortions. Specific digital processing techniques will be discussed for the rectification of: (1) video-system noises, (2) spacecraft video encoding nonlinearities, (3) spatial variations in vidicon sensitivity, (4) system geometric distortions, and (5) system resolution limitations.

MARINER MARS 1969 CAMERA SYSTEM

The Mariner Mars 1969 camera-system design evolved out of television experiment goals, state-of-the-art hardware capabilities, and Mariner project constraints as discussed by Leighton and Murray [1971]. The result was a vidicon-based digital camera system, similar to that used on the Mariner Mars 1964 mission, but with a significantly increased image format. More important in terms of the image-processing task, however, was the manner in which the data were processed and digitally encoded for

transmission to earth. In accommodating the low visual contrast of the Martian surface, the recovery of photometric information was made much more difficult and indeed impossible without digital processing of the images.

The Mariner 1969 video data were encoded and recorded within the television and data-storage subsystems (TVS and DSS) on board the spacecraft in a complicated manner, as discussed in detail by *Danielson and Montgomery* [1971]. The essential characteristics of the various types of picture data returned by the spacecraft are summarized here in terms of their effects on image processing. A simplified diagram of the flow of data in the Mariner camera system is shown in Figure 1. Each camera scanned a basic raster consisting of 945 picture elements per line and 704 lines per picture. Pictures were alternately read out of the low-resolution A camera and the high-resolution B camera at 42-sec intervals. For each such picture produced by the cameras, three separate encoded versions were transmitted to earth: a composite analog video (CAV) picture, a digital video (DV) picture, and an every twenty-eighth (ETE) digital picture.

The CAV pictures consist of the fully sampled

raster with each picture element digitized to 6 significant bits. Prior to the digital encoding of the CAV pictures, the amplitude-modulated camera output signal was processed through an automatic-gain-control amplifier (AGC) and a cubing amplifier to emphasize low-contrast detail, and was recorded on the analog tape recorder. The dynamic amplifier gains were not recorded.

The DV pictures consist of every seventh picture element along each scan line linearly encoded to 8 significant bits but with the 2 most significant bits (MSB) truncated prior to transmission. In a separate engineering-telemetry data stream, statistical information was transmitted for every block of 32 television lines indicating independently the dominant state for each of the MSB's. Of the 134 possible DN elements per line, the central 26 were used to transmit nonvideo science data thus forming a 'data bar' in the middle of the DV pictures.

The ETE pictures consist of every twenty-eighth picture element along each scan line linearly encoded effectively to 6 significant bits, but with the two MSB's truncated prior to transmission. These ETE data provide coverage in the 'data bar' of the DV pictures and, together

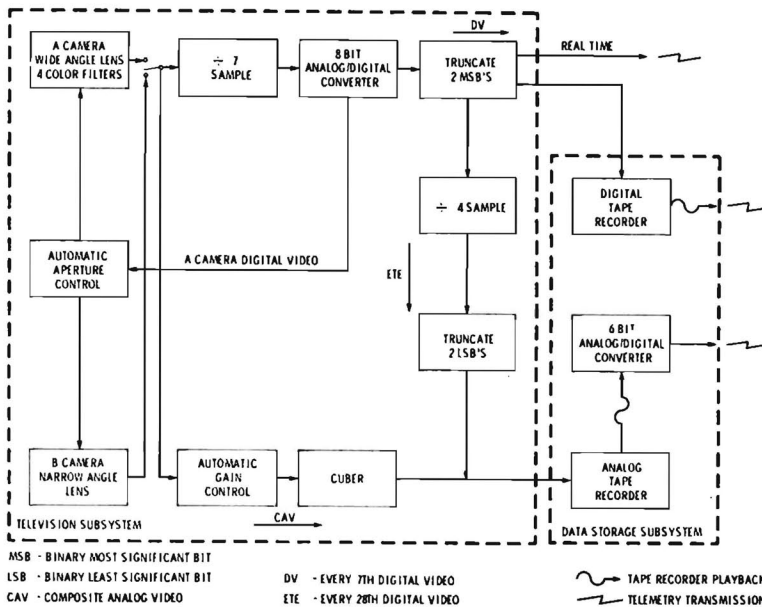


Fig. 1. A simplified block diagram showing the derivation, processing, and storage of the three Mariner 1969 video-data streams on board the spacecraft.

with the DV data, give information relative to the nonlinear effects of the AGC and cubing amplifiers on the CAV data. The time constants of the AGC amplifier were chosen so that the gain would change only very slowly over the every-seventh spacing of the DV samples.

A sample of the three spacecraft data streams is shown in Figure 2 along with the results of removing the AGC and cubing amplifier effects on the ground.

Operationally the camera system had two modes: far encounter (FE) and near encounter (NE). Because the planet would not fill the field of view as the spacecraft first approached Mars, the automatic-gain-control amplifier would adjust itself largely on the basis of black space, thereby causing saturation of the illuminated planet data. Thus in the FE mode the AGC amplifier was locked with a fixed gain. The cubing amplifier remained operational. Because of the small, slowly changing image size in far encounter, the low-resolution A-camera pictures were not

recorded at all, and the B-camera pictures were recorded only every 20 to 60 min.

In the NE mode, since the planet would change in brightness from limb to terminator, the gain controls were necessary. The NE mode had both the AGC and cubing amplifiers operating. Both A- and B-camera pictures were recorded consecutively in the near-encounter mode.

OBJECTIVES AND STRATEGY FOR MARINER IMAGE PROCESSING

The Mariner 1969 television experiment objectives included wide-ranging investigations of Mars and required processing of the television data to achieve (1) maximum equality image displays suitable for photointerpretation, and (2) maximum-quality image data for photometric and geometric measurements. The complexities of the Mariner camera system necessitated a correspondingly complicated processing procedure.

The image-processing task breaks into two

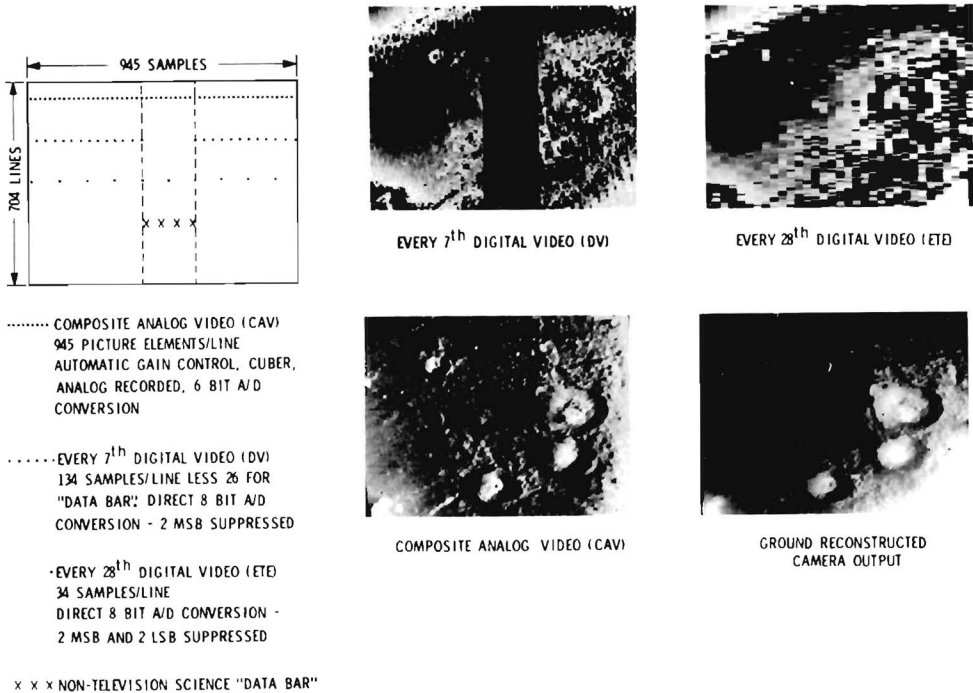


Fig. 2. A diagram and examples of the frame formats for the three on-board processed spacecraft video streams as well as the result of ground reconstruction of the photometric reference for the composite analog video. The pictures shown are of frame 7N12, and the sparsely sampled digital video pictures are filled out to full frames by repeating each sample 7 and 28 times, respectively.

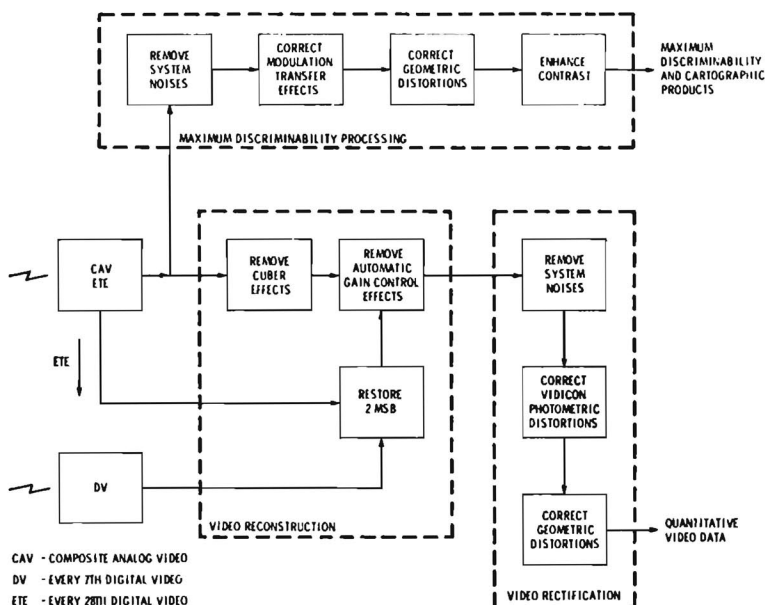


Fig. 3. A flow diagram for the ground processing of the three spacecraft video streams.

major subtasks: reconstruction and rectification. Video reconstruction consists of combining the three data streams (CAV, DV, ETE), restoring the missing most significant bits, and removing the nonlinear photometric effects of the AGC and cubing amplifiers. This step generates video data as they existed coming out of the camera heads. Video rectification then takes into account the various sensor distortions inherent in any television system, correcting them based on detailed calibration data. In the case of slow-scan vidicon systems, such as flew on Mariner, these distortions include system noises, residual image, sensitivity nonuniformities and nonlinearities, geometry distortions, and resolution limitations. A discussion of the calibrations performed on the Mariner camera systems is presented by *Danielson and Montgomery* [1971].

At many points during this processing sequence, images are produced depicting Mars in a variety of ways useful to photointerpretation. These data, displayed with various types of contrast enhancement, constitute a set of 'maximum discriminability' pictures. A collection of near-encounter maximum discriminability photographs is presented by *Dunne et al.* [1971].

The over-all flow of the three types of spacecraft video data through the digital processing

system is shown in Figure 3. Descriptions of the various functional blocks are presented in the subsequent sections.

The digital computer with its inherent flexibility and precision was the only feasible approach to solving the Mariner 1969 image-reconstruction and rectification problems with the massive amounts of data involved. Most of the camera effects were highly nonlinear, and in many ways each frame had unique problems associated with it, such as in the restoration of most significant bits to the digital video and the removal of automatic-gain-control effects. In very few instances was it possible to set up the processing in a 'production' mode. Much human interaction was required along the various steps.

The processing was accomplished in the Image Processing Laboratory of the Jet Propulsion Laboratory using an IBM 360/44 computer primarily and a much larger IBM 360/75 for the noise-removal portions requiring large Fourier transformations. The Image Processing Laboratory 360/44 machine is dedicated to image processing work and has a variety of peripheral image-display and scanning equipment, including an interactive console allowing direct human control over processing parameters.

A special software executive has been developed for the machine that simplifies job-control definition and that provides a highly efficient input/output processor for handling the large data files.

SYSTEM-NOISE REMOVAL

The practical limit to all quantitative or photointerpretive measurements on a properly encoded image is the presence of noise. Enhancement processes such as filtering to improve image resolution can sharpen features only at the expense of over-all signal-to-noise ratio. For these reasons, one of the most important initial steps in digital image processing is the suppression of noise, so that subsequent en-

hancement and restoration processing can be performed on maximum signal-to-noise ratio imagery to achieve optimized results.

Many noise sources exist in imaging systems ranging from random, wideband shot and thermal noises to highly structured periodic noises. Furthermore, in situations such as space photography, it is generally not possible to obtain multiple imagery in order to use frame-averaging techniques. The precise separation of any noise from the composite video of a single frame must be based on one or more quantifiable characteristics of the noise signal that distinguish it uniquely from the other video components. In most real situations one has only statistical information about the various components of

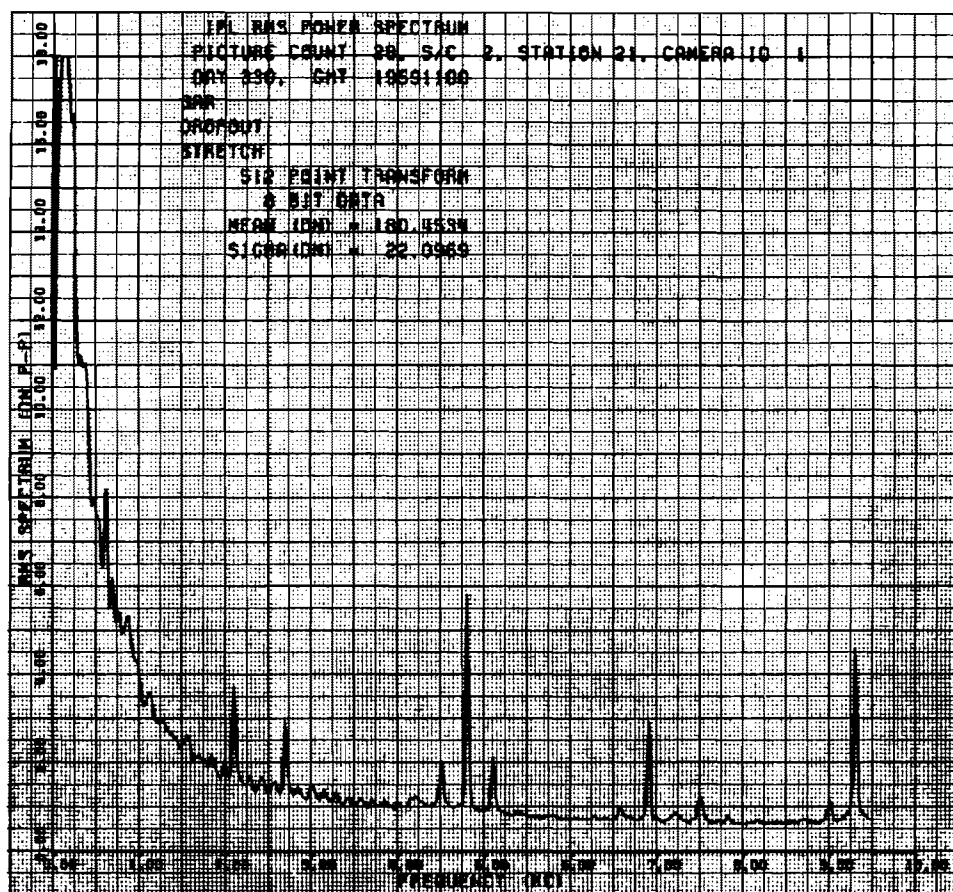
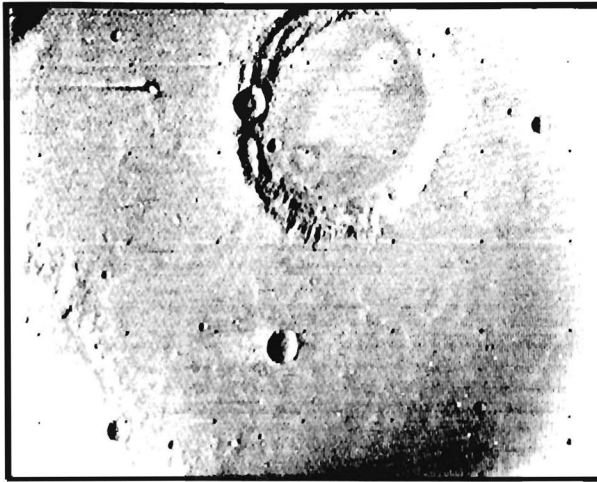


Fig. 4. A digitally computed Fourier power spectrum of a lunar test scene photographed by the Mariner 6 camera B in a prelaunch spacecraft test. The power spectrum was computed from the one-dimensional scan output of the camera.



FLIGHT PICTURE

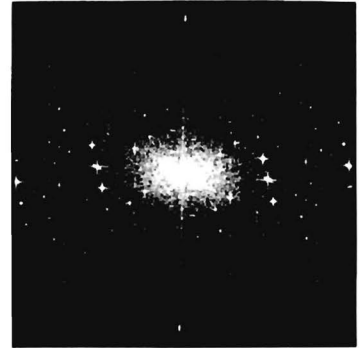
TWO-DIMENSIONAL FOURIER
TRANSFORMATION

Fig. 5. An example of a two-dimensional Fourier transformation of Mariner 6 camera B flight picture 6N18. The absolute spectrum amplitudes are displayed as shades of gray, increasing from black to white. Zero spatial frequency is in the center of the transform picture. Positive and negative horizontal spatial frequencies are displayed to the right and left of center, respectively, and positive and negative vertical spatial frequencies are shown above and below.

the total video signal and thus, even at the theoretical limit, their separation is approximate. This is certainly true in the data output of spacecraft video systems, where the dominant signal represents a complex natural scene. The essence of video noise removal is to isolate and remove the various identifiable and characterizable noise components as rigorously as possible, so as to do a minimum of damage to the actual video data. In most cases, the errors introduced to the real signal by the removal process, while small, vary from point to point and are impossible to measure meaningfully, since very little is known in detail about the scene being photographed and the efficacy of removal is data dependent. In the following, the removal of three different types of structured noise will be described, including periodic, long-line, and spike noises.

Periodic noise removal. In electronic video systems, a common noise problem arises from the coupling of periodic signals related to the raster-scan and data-sampling drives into the low-signal portions of the video-handling electronics. These noises are generally introduced when the video scene is represented by a one-dimensional temporal signal. Because of the periodicity of this type of noise, a useful method

for characterizing it is in terms of a Fourier decomposition. A one-dimensional digital power spectrum of a test scene photographed by a Mariner Mars 1969 camera is shown in Figure 4. The power spectrum clearly shows a smoothly varying background decreasing in amplitude with increasing frequency and representing the average scene spectrum on which is superimposed a number of narrow spikes. These spikes are the various components of the periodic noises present in the Mariner system and are related to multiples of the 2400-Hz spacecraft power-supply frequency.

For typical spacecraft systems, these periodic noises exhibit phase coherence over times that are long compared to the frame time of the camera. For this reason, when the two-dimensional image is reconstructed, the periodic noise appears as a two-dimensional pattern exhibiting periodicity not only along the scan lines, but perpendicular to them as well. If one computes a two-dimensional Fourier transform of a reconstructed picture, as shown in Figure 5, this two-dimensional structure becomes evident. Again, the actual scene spectrum appears as a continuum falling off in amplitude toward high spatial frequencies, and the noise components appear as well-defined two-dimen-

sional star-like spikes. The continuum is irregular in the case of the two-dimensional transform because there is no averaging, as in the case of the one-dimensional power spectrum.

Because the noise as well as the scene exhibit two-dimensional correlation, a more precise removal can be achieved by filtering the noise from the two-dimensional Fourier space than from the one-dimensional space. This can be seen by considering the effects of one-dimensional filtering as observed in the two-dimensional transform space. Since the removal of a one-dimensional horizontal frequency component

is done without regard to its vertical variation, the corresponding spectral components removed in two-dimensional frequency space lie in a vertical bar. Since the noise component is contained in a restricted region along the bar, a large amount of video signal is unnecessarily removed.

Removing the two-dimensional spikes, one achieves a first-order cleanup of the periodic noise components. By this method only the portion of the component spectral spikes can be isolated that protrude above the video spectrum continuum, without unduly distorting

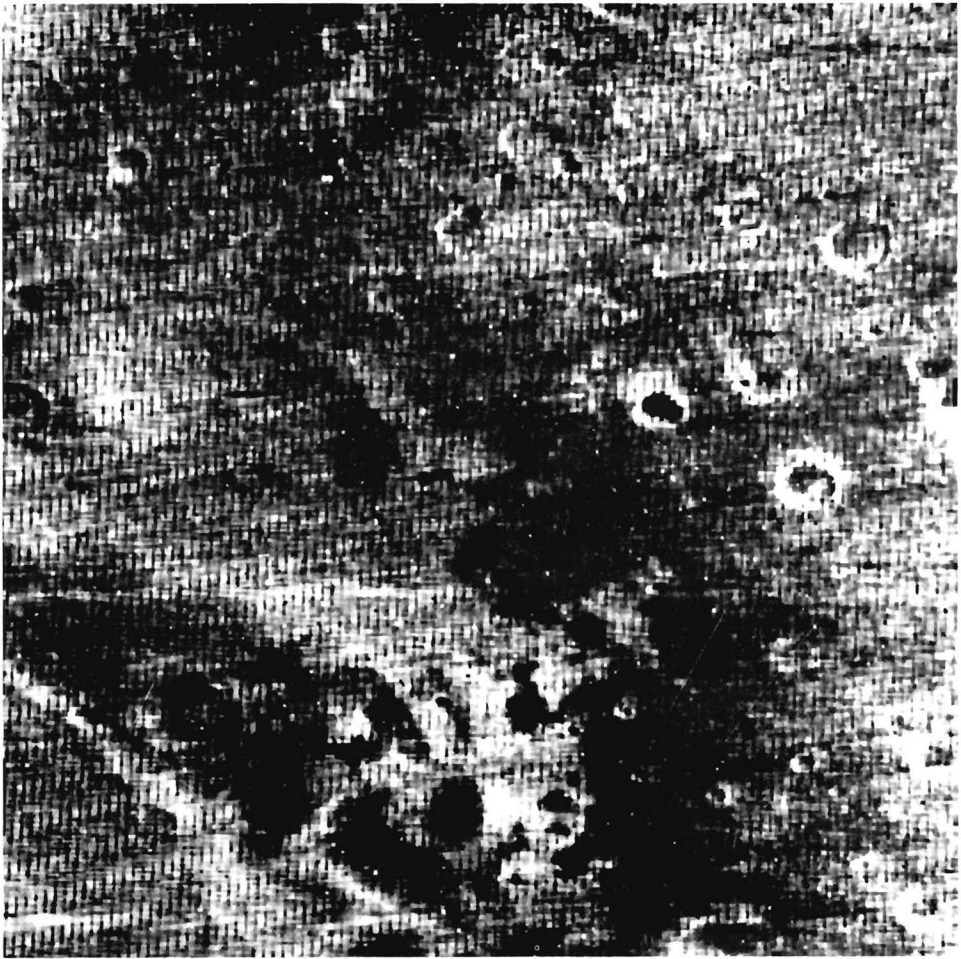


Fig. 6. A portion of Mariner 6 picture 6N13 (Meridiami Sinus) with only a contrast enhancement applied to the raw composite analog video received from the spacecraft. This segment has been enlarged two times to make the system noises readily visible.

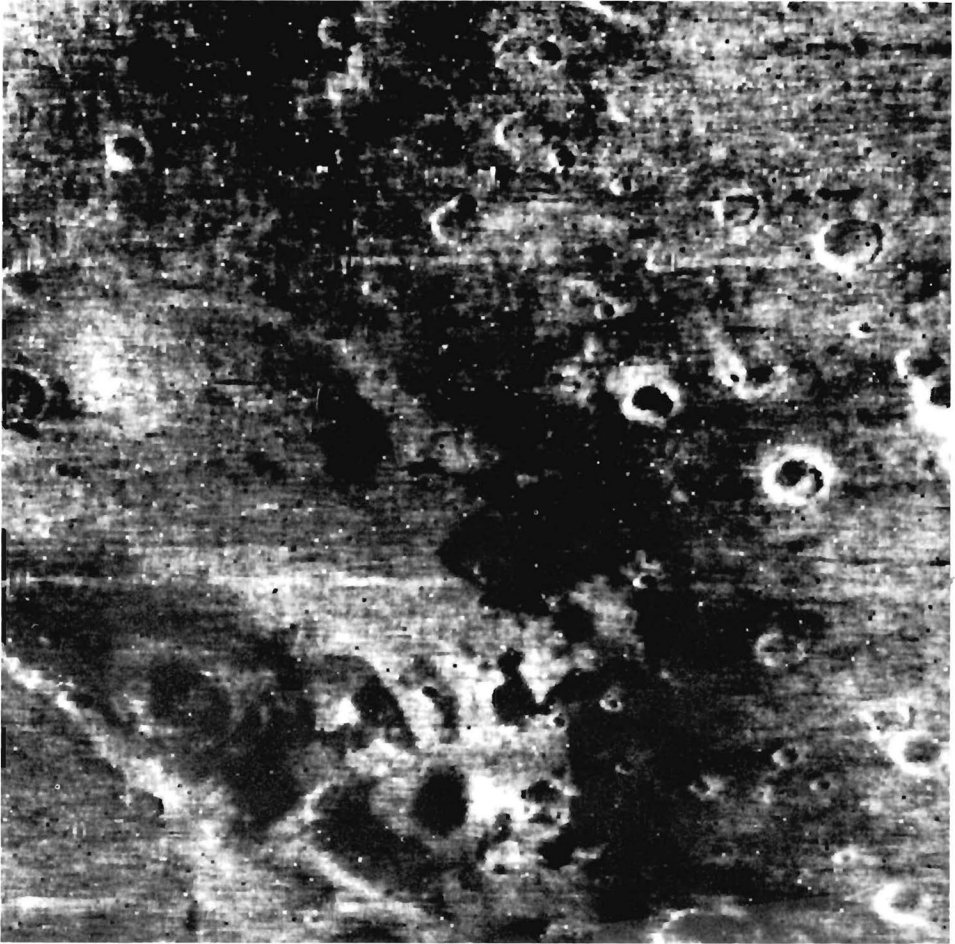


Fig. 7. The result of removing the periodic noises from the segment of 6N13 shown in Figure 6. Note that the short horizontal analog tape recorder dropout noises are now clearly visible.

the video signal. As can be seen in the power spectrum of Figure 4, the spikes have skirts extending below the continuum. These skirts represent a subtle local modulation (generally amplitude modulation) of the basic noise pattern as might occur with amplitude dependence or saturation effects on the noise signal. These cannot be readily isolated by frequency-space filtering. A more effective approach is to determine a local modulation coefficient for the idealized noise pattern derived from careful two-dimensional filtering. This coefficient is typically slowly varying relative to the resolution limits of the camera. The criterion that is used

for determining the local modulation coefficient is to minimize the variance, over a local region, of the noisy signal minus a variable fraction of the idealized noise pattern. If N_{ij} is the noisy image, n_{ij} is the idealized noise pattern, A_{ij} is the local modulation coefficient, and σ_{ij}^2 is the 'cleaned-up' signal variance for the local region of dimension M , the definition of local signal variance

$$\sigma_{ij}^2 = \frac{1}{(M+1)^2} \sum_{k=-M/2}^{M/2} \sum_{l=-M/2}^{M/2} [(N_{i+k, j+l} - A_{ij} n_{i+k, j+l}) - (\langle N \rangle_{ij} - A_{ij} \langle n \rangle_{ij})]^2$$

is used. The bracketed terms are average values defined for any matrix m_{ij} to be

$$\langle m \rangle_{ij} = \frac{1}{(M+1)} 2 \sum_{k=-M/2}^{M/2} \sum_{l=-M/2}^{M/2} m_{i+k, j+l}$$

By using the minimization condition

$$d\sigma_{ij}^2/dA_{ij} = 0$$

one derives the expression

$$A_{ij} = \frac{\langle [N_{ij} - \langle N \rangle_{ij}] [n_{ij} - \langle n \rangle_{ij}] \rangle}{\langle [n_{ij} - \langle n \rangle_{ij}]^2 \rangle}$$

which defines a modulation coefficient for each point in the picture in terms of the noisy image and idealized noise pattern. The dimension M of the local area used to determine the coefficient A_{ij} for each point is chosen on the basis of the spatial frequency bandwidth appropriate for A_{ij} .

The idealized noise pattern is generated by bandpass filtering the two-dimensional Fourier transform of the noisy image. All elements of the image transform, except those at which spikes caused by noise occur, are set to zero. The idealized noise pattern is then obtained by

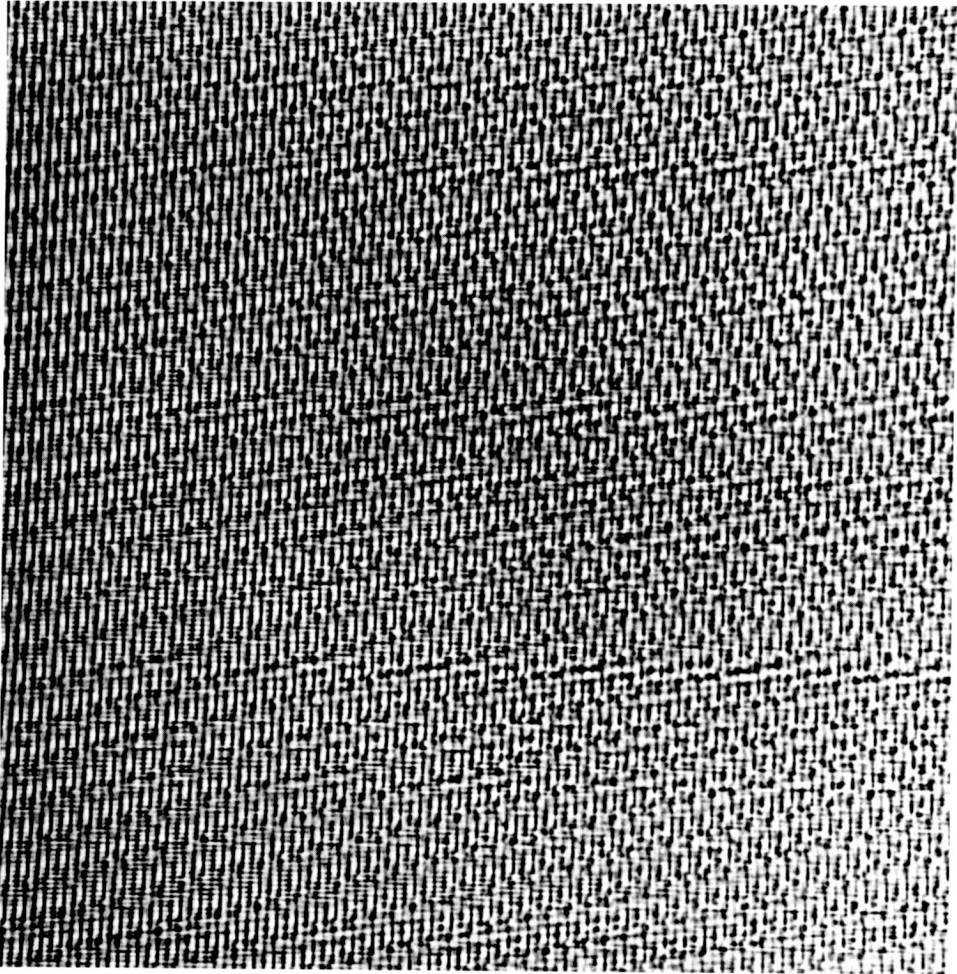


Fig. 8. The complicated periodic noise pattern removed from Figure 6 to obtain Figure 7. Note the nonuniformity of the pattern from left to right resulting from the complex phase relationships between spectral components.



Fig. 9. The result of removing the analog tape recorder dropout noises from picture 6N13 after the periodic noise removal shown in Figure 7. Note that the black and white spike noises scattered through the picture are now clearly visible.

computing the inverse Fourier transform of this filtered image transform.

To determine at which elements of the transform noise spikes occur, the amplitude of the transform function is computed. Since this function consists of high-amplitude noise spikes superimposed on a continuum that is characterized by very high amplitudes at low spatial frequencies decreasing to quite low amplitudes at high frequencies, it is possible to identify noise spikes as those elements for which the amplitude exceeds that of the continuum by a specified amount. An approximation to the continuum is generated by low-pass filtering

or by averaging the amplitude of the transform function over a nine by nine area about each element. This average is then subtracted from the original to yield a detrended transform consisting of noisy spikes on a relatively uniform amplitude background. A threshold value is specified, and the Fourier transform of the idealized noise pattern is obtained by setting to zero all points of the image transform for which the corresponding point in the detrended transform falls below the threshold.

Although the technique was very effective in generating an idealized noise pattern, it proved to be too time consuming to be implemented

on all the Mariner 1969 images. A procedure was therefore developed that takes advantage of the fact that the spatial-frequency components of the coherent noise varied only slightly in position between successive frames and eliminates the need to compute an averaged amplitude of the transform function for each image. From groups of approximately eight sequential frames, typical images were selected. By using the previously described technique to isolate the noise spikes in the transform-amplitude function of the selected image, a mask was generated by constructing rectangular areas about the

isolated spikes. Noise spikes were identified for all images in the group as those transform-amplitude elements that fell within the rectangles of the mask and had amplitudes greater than a given threshold.

An obvious deficiency of this procedure is that in the low-frequency areas of the transform where the amplitude of the continuum was greater than the specified threshold, image information could be incorrectly identified as noise spikes. However, care was taken in these regions to assure that the number of misidentified elements was very small, and it



Fig. 10. The result of removing the spike noises from picture 6N13 after the periodic and dropout noise removal shown in Figures 7 and 9. Note in comparison with the raw picture in Figure 6 that terrain features of considerably higher resolution are discernable in Figure 10.

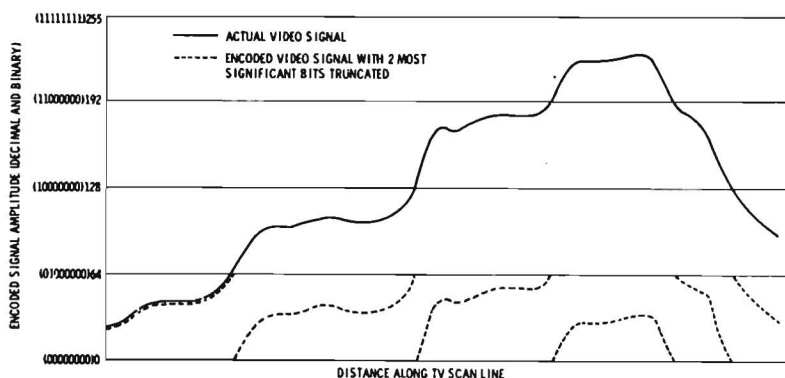


Fig. 11. An example of the effects of truncating the two most significant bits from an eight-bit binary encoded line of video data. As the true signal crosses the quadrant boundaries of the encoder dynamic range, the required amplitude information is lost, forcing all segments of the truncated signal to lie in the lowest quadrant.

was found that the abbreviated technique did not introduce a significant amount of image information into the idealized noise pattern.

The results of applying these techniques to remove the periodic noise components from the Mariner 6 picture shown in Figure 6, are apparent in Figure 7. The complicated periodic noises that were extracted are seen in Figure 8.

Long-line noises. A variety of mechanisms can produce long-line or streak noises in television images such as gain variations, data outages, and analog-tape-recorder dropouts. This type of noise, caused by tape-recorder dropouts in the case of Mariner 1969, becomes apparent as horizontal streaks in Figure 7 with the removal of the periodic noise.

The characteristic that distinguishes streak noises from the actual scene is their linear correlation along the scan-line direction and the lack of correlation in the perpendicular direction. This distinction is not complete, however, since linear features are present in some natural scenes, and statistically they will be oriented occasionally along the line direction. The problems of data-dependent noise removal are exemplified by this case since major damage to the true video signal may result in particular localized regions that contain scene components resembling the noise.

The technique developed to correct for these streak noises is to compare the local average intensity value of lines adjacent and parallel to the streaks with the average value of the streak itself, and to apply a gain factor to account

for any differences. A multiplicative rather than an additive correction is applied because the physical origin of the noise (magnetic tape dropouts) is multiplicative. Since the correlation between points in a picture decreases with increasing separation, a linearly decreasing weight is applied to more distant local lines in determining the surrounding average. If N_{ij} is the noisy picture (j is the index along the direction of the streak noises) and G_{ij} is the corrective gain to be applied to the point (i, j) , the expression

$$G_{ij} = \frac{\sum_{k=1}^P (P - k + 1) [\langle N \rangle_{i+k,i} + \langle N \rangle_{i-k,i}]}{P(P + 1) \langle N \rangle_{ij}}$$

is used where P is the number of adjacent lines used above and below the streak and the average values are defined by

$$\langle N \rangle_{ij} = \frac{1}{Q + 1} \sum_{k=-Q/2}^{Q/2} N_{i,j+k}$$

In this latter expression, Q is the low-pass-filter dimension along the direction of the streaks and is determined by the lengthwise correlation of the long-line noise. The dimension P is determined by the perpendicular correlation.

A further refinement is used in determining the numerator of the gain-determining equation. The numerator is computed as shown, but then a 'majority rules' logic is applied so that terms deviating significantly from the average are eliminated from determining the average on

a second pass. This algorithm is a refinement of the long-line filter described by *Nathan* [1966].

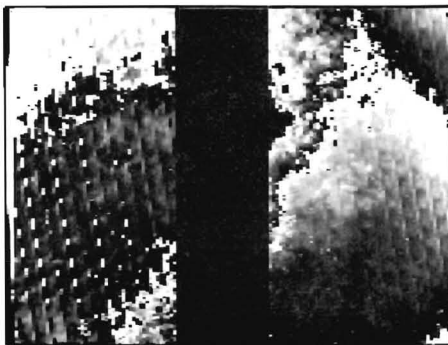
The result of correcting for the streak noises in Figure 7 is shown in Figure 9. It should be emphasized that this correction is particularly data dependent in its effect and although closer to the truth in the large, may introduce artifacts in the small.

Isolated spike noises. The occurrence of a bit error in telemetering digital video data or the presence of temporally sharp spikes of noise from the analog electronics can cause isolated picture elements to deviate significantly from the surrounding data. The removal of the periodic and streak noises illustrated in Figure 9 reveals this additional noise component consisting of black and white spikes. The character-

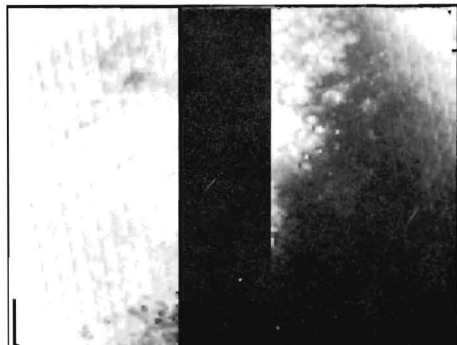
istic that distinguishes these spike noises from the actual video is the fact that because of resolution limitations of a Nyquist-sampled video system, the variation from one picture element to another of the true signal is limited.

The logic used to remove these spike noises is very simple. Each picture element is examined and if it is significantly above each of its neighbors or significantly below its neighbors, it is replaced by the average neighboring intensity. The results of applying this correction to the remaining spike noises in Figure 9 are shown in Figure 10.

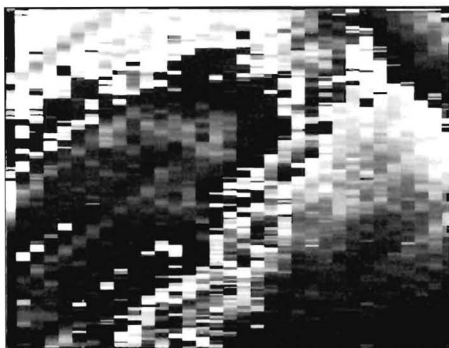
In this case, as with the long-line noise, the removal process is not perfect and restores only an approximation to the true video data that was masked by the noise. The threshold parameters were chosen so that only the relatively



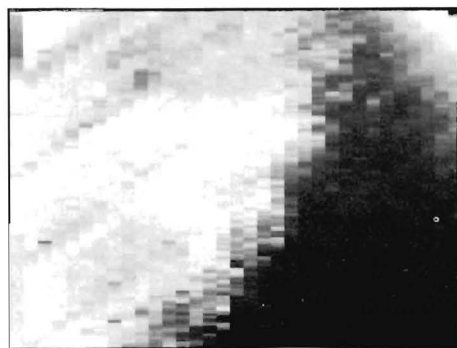
RAW DV-2 MSB MISSING



PROCESSED DV-2 MSB RESTORED



RAW ETE-2 MSB MISSING

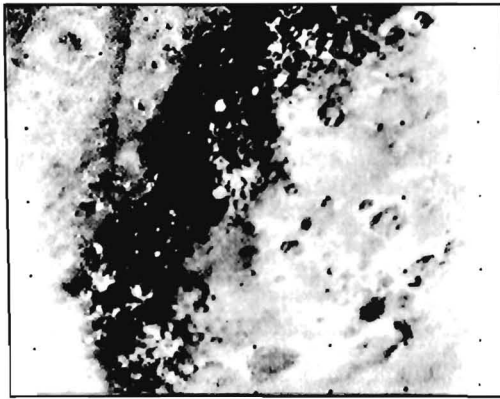


PROCESSED ETE-2 MSB RESTORED

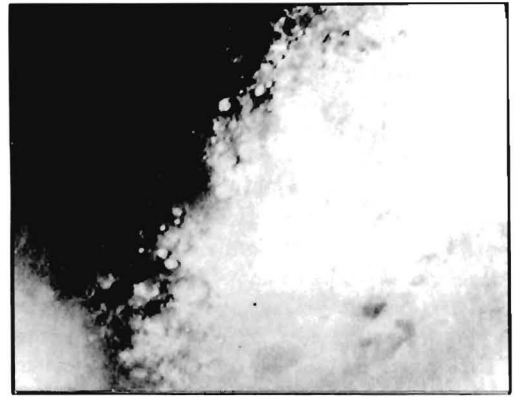
DV-EVERY 7th DIGITAL VIDEO

ETE EVERY 28th DIGITAL VIDEO

Fig. 12. The results of restoring the two most significant bits to the two digital video frames received for Mariner 7 camera A picture 7N13. The frames have been expanded to the full camera format by repeating each sample 7 and 28 times, respectively. The diagonal streaks are caused by the camera-system noises aliased because of the sparse sampling.



RAW CAV-CUBER & AUTOMATIC
GAIN CONTROL EFFECTS PRESENT



RECONSTRUCTED CAV-CUBER & AUTOMATIC
GAIN CONTROL EFFECTS REMOVED

CAV-COMPOSITE ANALOG VIDEO

Fig. 13. The result of removing the effects of the cubing and automatic-gain-control amplifiers from picture 7N13 using the results of the most significant bit restoration shown in Figure 12. Note that the on-board processing had the desired effect of enhancing low-contrast surface detail both on and off the polar cap in the raw composite analog video.

few points obviously in error were corrected, and any reasonably probable signal variation was left unaltered.

A comparison of Figures 6 and 10 shows a dramatic improvement in signal-to-noise ratio by using the digital computer to isolate and remove various structured noise components from the raw video. This type of processing, although preliminary to further restorative steps, itself produces an enhancement that allows analysis of surface detail closer to the resolution limits of the camera system. Techniques for removing noises from video are of widely varying character and in some cases strongly video-system and data dependent.

NONLINEAR ENCODING RECONSTRUCTION

The three types of encoded video data transmitted from the Mariner 1969 spacecraft to earth have a complex relationship to the video-data output from the camera sensors. Whereas the distortion characteristics of the sensors are constant with time and are calibratable, the properties of the encoding system are dynamic, and they adapt to the unique luminance variations of the scene being photographed. A major aspect of the Mariner image-processing task was the extraction of the implicit information about the encoding-system effects from the

three data streams and its application to reconstruct the video signal at the sensor output for subsequent correction of calibrated vidicon distortions.

The steps required for this video reconstruction are shown in Figure 3. The two sparsely sampled data streams (every seventh, DV, and every twenty-eighth, ETE) must have the truncated two most significant bits restored. The fully sampled analog data (CAV) must have the cubing-amplifier effects removed. The final step then is to combine the three processed streams to reconstruct the dynamic gain applied by the automatic-gain-control amplifier (AGC) and to produce a fully sampled image as it appeared directly at the camera sensor output.

Restoration of the most significant bits. The binary encoding of a picture element represents a series approximation to the camera signal output at that point with the most significant (or high-order) bits giving coarse amplitude information and the lower-order bits progressively refining the approximation. The truncation of the two most significant bits (MSB) from such a binary code introduces an ambiguity into the gross amplitude of the resulting number. As shown in Figure 11, each truncated data point could lie in any of four equal quadrants of the dynamic range of the digitizer. From the context

of the slowly varying signal shown in Figure 11, however, it is intuitively evident that relative MSB transitions occurred at the abrupt discontinuities of the MSB truncated dashed curve. As the activity of the signal increases, i.e., as large amplitude changes in the true signal take place over shorter and shorter distances, it becomes more and more difficult to reassign unambiguously most significant bits to the truncated data. The choice of this bit-truncation data-compression scheme was based on the low-contrast character of Mars and the correlation from picture element to picture element imposed on the camera output by the resolution limitations of the system. For pictures in which the video signal is confined over-all to fewer than four quadrants, i.e., for very flat scenes, there remains an amplitude ambiguity for the whole picture even after the relative MSB transition discontinuities are repaired. Such uncertainties are resolved on the basis of the statistical sampling of the state of each of the image-data MSB's that were returned in the engineering telemetry. These additional data measure independently whether each MSB was predominantly on or off for each 32-line block in the pictures.

Although the high-frequency noises in the flight images significantly complicated the MSB restoration process and necessitated considerable human interaction with the computing, it has

been possible, with very few exceptions, to restore unambiguously the missing significant bits to the Mariner flight digital streams. The algorithm that was used searches the raw digital data for abrupt transitions, such as appear in Figure 11, and introduces most significant bits so as to minimize the discontinuities. This search is done for each column independently, since the picture elements along the columns are contiguous and the columns are spaced 7 and 28 picture elements apart, respectively, for the DV and ETE data streams. Clearly, if the absolute difference between adjacent raw intensities is either large or small, one can say with confidence that a MSB transition has or has not occurred. If the difference is of intermediate magnitude, the occurrence of a transition is ambiguous. The locations of such ambiguities are logged for each column for later use in resolving the MSB pattern for the entire frame.

After processing all the columns of the picture in this way, approximate intensity continuity between adjacent columns is imposed to attempt to resolve remaining ambiguities. A starting column is chosen either manually or by automatically locating that column with the most quadrants present (but not exceeding four) and with the fewest ambiguities. This column is compared with those adjacent, and MSB's are changed between ambiguous transitions to produce the smoothest result. This process



RESIDUAL IMAGE PRESENT

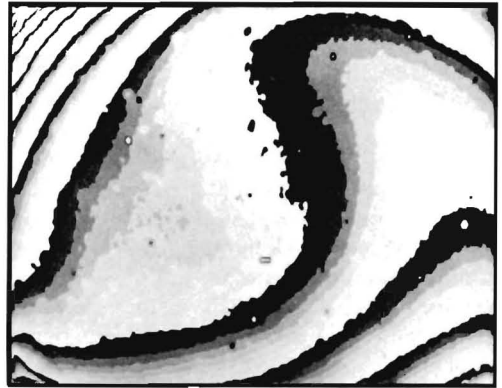


RESIDUAL IMAGE REMOVED

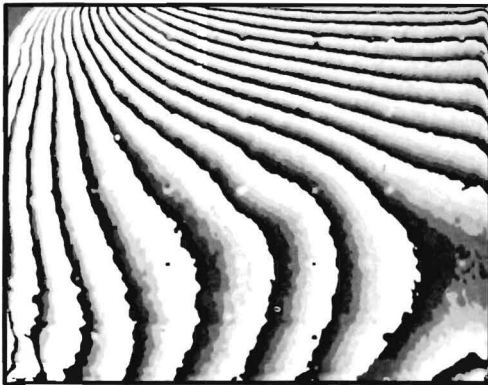
Fig. 14. The result of removing the limb residual image from Mariner 7 camera B picture 7F62. Since successive camera exposures were not transmitted in the far-encounter sequences, the picture shown was used to model its own residual image.



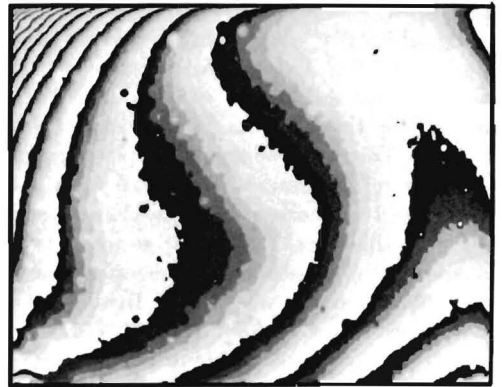
100 FOOT-LAMBERTS



400 FOOT-LAMBERTS



1600 FOOT-LAMBERTS



800 FOOT-LAMBERTS

Fig. 15. A sequence of computer contoured preflight flat-field calibration frames for Mariner 6 camera A showing the spatial evolution of photometric sensitivity contours with increasing input target luminance. Contouring was achieved by truncating five of the eight encoded bits so that each black-to-white contour represents an output-signal change of eight intensity levels.

continues for the entire picture to reconstruct the MSB pattern based on two-dimensional continuity.

In many cases this semiautomatic MSB restoration process produces quite satisfactory results, but predictably in very high-contrast scenes such as near the polar cap or in very noisy pictures such as in higher-gain states, manual intervention is required to correct isolated and localized errors. This manual correction requires printing of the numerical picture-intensity values and a decision for a correction by an analyst on the basis of interpretation of the image content.

At this point final corrections to the restored MSB's are made, removing residual errors

around the sharp, high-amplitude geometric rescan-pattern elements. These points are positioned on the sensor face to calibrate electronic geometric distortion changes. They are of small size and cause video-signal transitions in some cases between adjacent picture elements of more than one quadrant, thereby making MSB restoration difficult. Additionally, the small number of remaining isolated MSB ambiguities caused by spike noises are resolved by locally comparing the digital data with the highly approximate relative amplitudes derived from the fully sampled AGC output and assuming small AGC gain changes between adjacent CAV columns corresponding to those in the digital video.

An example of the raw DV and ETE data returned in picture 7N13 is shown in Figure 12 together with the result of the most significant bit restoration processing.

Correction of the cubing amplifier. The cubing amplifier introduces gain effects that are strongly amplitude dependent and that tend to emphasize the low-contrast, high-spatial-frequency detail of the signal produced by the AGC amplifier. The cubing amplifier is a wide-bandwidth device, hence its effects on adjacent picture elements can be considered independent. Furthermore its gain characteristic is fixed and does not adapt to the local signal properties as does that of the AGC amplifier.

The transfer characteristic of the cubing amplifier was measured prior to flight as part of the calibration procedure [Danielson and Montgomery, 1971]. Because in the far-encounter (FE) mode the AGC gain is fixed, the flight data provide the opportunity for an in situ calibration. This is accomplished by plotting, for a sequence of FE frames, the CAV intensity values against the corresponding ETE intensity values. In this plot the variation of planet luminance within the pictures generates points spaced along the transfer curve. Because the ETE data is returned without the MSB's present, the resulting plot consists of four segments with the breaks corresponding to the MSB transition points. It is straightforward to translate these segments to produce a continuous curve. The in situ measurements made in this way agree with the preflight data to within 2-3%.

The cuber-transfer curve derived from the flight data represents, for each spacecraft, a transfer table associated with each cubing amplifier relating binary-encoded input amplitudes with a corresponding output amplitude, and vice versa. These tables are used to remove the effects of the cubing amplifier. In the FE mode, since the AGC gain is fixed, this produces data as it appeared at the camera output. In the NE mode, on the other hand, this correction produces data as it appeared at the AGC amplifier output and requires the subsequent correction of the AGC effects.

Correction of the automatic-gain-control amplifier. The automatic-gain-control amplifier (AGC) applies a dynamic gain to the video signal in the NE mode with the intent of maintaining the locally averaged output-signal

amplitude at the steepest part of the cubing-amplifier characteristic. This guarantees that the maximum enhancement of the high-frequency components of the AGC output signal will result. These components, of course, represent the small, low-contrast surface features of interest to photointerpretation. The AGC amplifier is a highly nonlinear feedback device that uses a low-pass-filtered version of its output signal to continuously adjust its gain so as to maintain a constant output. The time constant with which AGC gain changes can occur is related to the bandwidth of the low-pass filter in the feedback loop and is chosen so only small changes are possible between every seventh and twenty-eighth samples.

Thus since the DV and ETE data with the restored most significant bits represent sample points at the input to the AGC amplifier, effective AGC gains can be determined at these points and interpolated for points in between to approximate the continuously varying AGC gain function. Linear interpolation is used because the presence of system noises in the data makes the gain calculations correspondingly uncertain. Higher-order interpolations would tend to emphasize these problems and introduce additional artifacts.

In photographs containing the limb, the sparsely sampled DV and ETE data give only a spatially step-like approximation to the true limb profile. This effect, coupled with the inaccuracy of the effective AGC gains that can be determined immediately off the limb in black space (both the digital data and the decubed data are near zero, since the limbs are very sharp), produces a correspondingly step-like result for the limb profiles corrected by the above method. This was corrected by applying the last uninterpolated gain value determined along each line on the planet side of the limb to the data in the neighboring limb transition. This approximation is consistent with the time constant of the AGC amplifier. The remaining black-space area off the limb was then set to zero, consistent with the undetectable intensities (zeroes) in the corresponding digital video. An example of the result of reconstruction on the previous picture 7N13 is shown in Figure 13. The photometric distortion introduced by the AGC/cubing-amplifier combination is evident in the region of the polar cap-desert interface

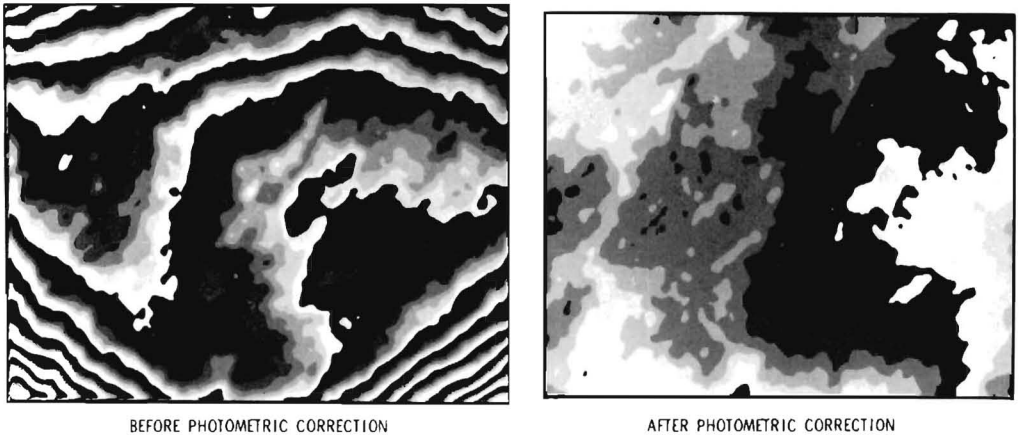


Fig. 16. A computer-contoured comparison of the average of all the Mariner 7 camera B flight pictures before and after correction of the vidicon sensitivity nonlinearities and spatial nonuniformities. Contouring was achieved as in Figure 15. The residual shading after photometric correction is subjectively consistent with expected phase-angle effects.

in the center of the picture. The dark band in this area is an artifact that reflects the dynamic response of the AGC. The reconstructed data represent video at the output of the cameras with all the nonlinear encoding effects removed.

RESIDUAL IMAGE REMOVAL

The vidicon tubes employed in the Mariner '69 TV camera systems were high-sensitivity storage tubes and therefore exhibited significant frame-to-frame image retention. It was determined early in the calibration data analysis phase that somewhere between 5 and 20% of the image corresponding to exposure N would persist in exposure $N + 1$. Visible residual images were observed under appropriate conditions, e.g., when a flat-field or very nearly featureless target was photographed following a high-contrast target. Several types of calibration data were collected to assist in the quantitative characterization of this phenomenon. A simple linear model was used to approximate the residual image effects. If $O_i(x, y)$ is the total camera output for frame i , and $S_i(x, y)$ is the camera output with no residual image effects, it was assumed that

$$O_i(x, y) = S_i(x, y) + A(x, y)O_{i-1}(x, y)$$

where $A(x, y)$ is a spatially varying retentivity coefficient.

Complex gray-scale targets were photographed in one orientation three times in succession, then rotated and photographed three more times. The targets were designed in such a way that a rotation of 90° resulted in an exposure change either up or down at each point in the image plane. By measuring camera output values in several of the pictures in the series described above, approximate retentivity coefficients were determined for the entire scanned area of the tube. Another type of data used to determine the spatial variation of retentivity within the scanned region of the vidicon target consisted of flat-field pictures taken in ascending and descending light-level sequences. A difference picture between a flat field exposed at luminance L preceded by a frame with luminance $L_1 > L$ and one also exposed at luminance L , but preceded by luminance $L_2 < L$ represents a 'map' of retentivity for that particular set of input luminance levels.

The complex gray-scale and flat-field measurements showed that, for the flight vidicons, the retentivity coefficient varies slowly across the scanned area, with an amplitude variation of as much as a factor of 2. Maps of residual image sensitivity for each camera, consisting of a retentivity coefficient for each image element, were constructed from these data. These retentivity maps were tested and demonstrated to effectively remove visible residual images observed during preflight calibration testing.

For a sequence of pictures taken by a camera, the appropriate map is applied as a modulation matrix to picture $N - 1$ of the sequence, so that an appropriate fraction of its intensity values can be subtracted from picture N at each image element to effect residual image removal.

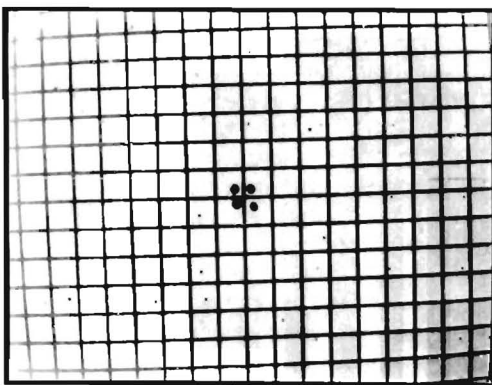
This approach has been used in the removal of residual images from preflight light-transfer calibration data and has been used in the removal of residual images from all flight data. In all except the Mariner 7 camera A, the preflight retentivity maps produced an effective removal of visible residual images from the flight pictures, with only an over-all amplitude-scale adjustment required in the retentivity maps for several cameras.

However, preflight calibration analysis indicated a gently sloping, nearly planar retentivity map for the Mariner 7 camera A vidicon. When this map was used in an attempt to remove residual images from Mariner 7 flight data, it was found to be inappropriate, and the spatial retentivity coefficient slope seemed no longer to exist. Although the difference between the flat-field and the sloping calibration retentivity surface was small, the difference between pictures 'corrected' using the two were visually distinguishable. The necessity to abandon the preflight Mariner 7 camera A retentivity map is disturbing, suggesting as it does that either a measured property of the vidicon had changed during flight or, alternatively, that the preflight measurements were inadequate. Photometric dis-

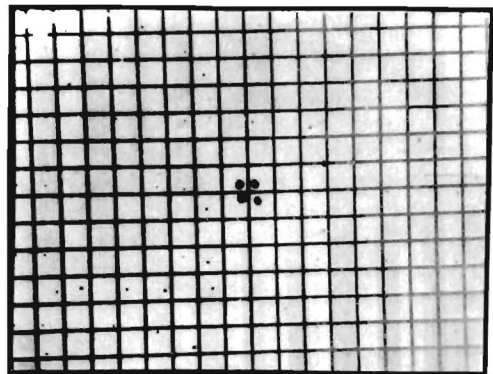
crepancies between pictures corrected by means of the flat and sloping version of the Mariner 7 camera A retentivity maps amount to 2-3%.

The removal of residual images from far-encounter (FE) data involves an additional complication because successive camera exposures are not available. Only widely spaced FE pictures were recorded so that the analog-tape-recorder capacity (33 pictures) would be optimally utilized as the planet image scale slowly changed during approach. Residual removal, then, requires a 'bootstrap' technique wherein each recorded frame is used to approximate the immediately preceding camera exposure and thence to remove the residual image from itself. Planet image changes caused by rotation during the 84 sec between camera exposures are less than two picture elements for the closest far-encounter pictures and were ignored within the accuracy of this approximation. Because of the size of the residual effect, the visible residual limb of the previous exposure provided a guide to translate and register each image with the residual of the preceding frame (the spacecraft guidance system caused slight shifts in the planet image from frame to frame). At this point the appropriate retentivity coefficient map was used to subtract the necessary fraction of the simulated preceding frame to remove the residual.

An example of the removal of the residual image from FE frame 7F62 is shown in Figure 14. The residual removal technique described greatly reduced the visibility of the residual



BEFORE GEOMETRIC CORRECTION



AFTER GEOMETRIC CORRECTION

Fig. 17. A comparison of the preflight geometric calibration grid target as photographed by the Mariner 6 camera A before and after correction.

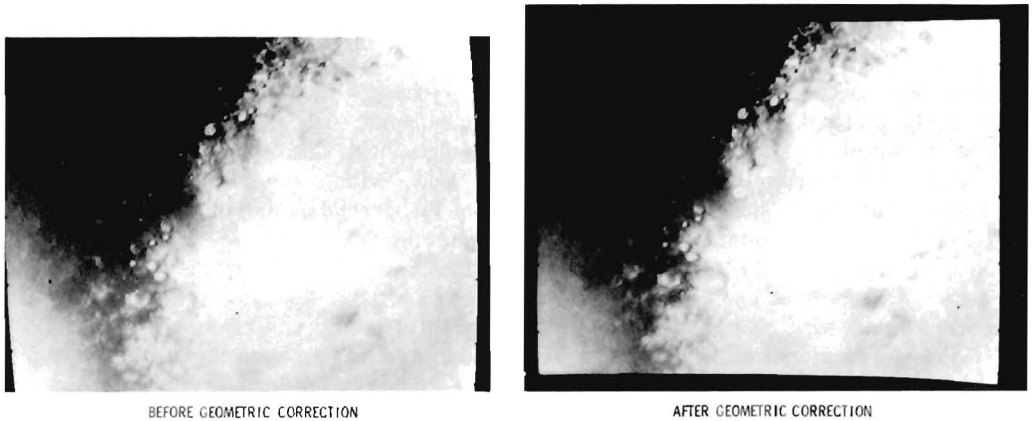


Fig. 18. A comparison of the results before and after correcting the camera-system geometric distortions for Mariner 7 camera A picture 7N13. Note the large relative corrections necessary in the upper left and lower right corners.

image component. In general, residual removal was possible to approximately 3% uncertainty in the corrected intensity value.

PHOTOMETRIC DECALIBRATION

After residual image removal is completed, the pictures still retain the 'signature' of non-linear and spatially varying light-sensitivity properties of the vidicon. Each of the vidicons utilized in the Mariner missions was calibrated extensively to determine, as a function of position in the frame, the relationship between input luminance and camera output signal. This included measuring the system light-transfer properties for each of the camera filters and as a function of camera temperature. In effect each element of the 945 sample by 704 line raster is treated as a tiny photometer with unique light-transfer properties. These photometric calibration data are organized and stored in such a way that when each picture element in a flight frame is to be corrected, the appropriate calibration curve for that element is located, the recorded camera-output signal is converted to the actual scene luminance, and the result is stored in the output corrected image.

Danielson and Montgomery [1971] describe the collection of the calibration data on which the photometric correction of the Mariner pictures is based. These consist of a series of 'flat-field' pictures generated by exposing each camera to a spatially uniform stimulus at a variety of accurately measured luminance values over the

dynamic range of the system. Contoured examples of the resultant pictures for a Mariner 6 flight camera are shown in Figure 15. The gradients evident in these pictures (8 intensity levels out of 256 correspond to one black-to-white cycle) result from spatial sensitivity variations in the vidicon target (input fields were flat to within 2-3 equivalent levels). Data of this type were collected in a number of calibrations for each camera filter and gain state, and over a range of operating temperatures designed to include expected encounter temperatures. Examination of the thermal data showed that the shading characteristics varied in such a way that no single temperature correction coefficient could be applied over the entire vidicon surface, but rather each image element required its own correction factor. Accordingly, encounter temperature-calibration files were generated by combining cold and room-temperature calibration data on a picture-element by picture-element basis, with a different interpolation factor applied to each image element.

Preliminary examination of the corrected flight data indicates that this approach has been successful, to a first order at least, in removing vidicon shading in the photometrically corrected pictures. As an example, Figure 16 is a contoured version of the average of all Mariner 7 camera B pictures that were reconstructed by application of the AGC correction (again, one cycle corresponds to 8 DN). A similarly contoured version of these same pictures after photometric cor-

rection is also given in Figure 16. Similar results have been obtained with the other flight cameras. Residual shading in all cases is coincidental with expected photometric gradients due to phase-angle effects, although analysis is not yet complete with regard to a quantitative match and residual errors. Cross correlation between photometrically decalibrated data obtained from the various cameras has, however, indicated the presence of large (20–30%), unexplained inconsistencies, particularly at low light levels. These comparisons have been made between A and B cameras on the same spacecraft in areas of overlap, and between Mariner 6 and 7 B camera (far-encounter) views of the same surface features viewed under approximately the same conditions. The resolution of these anomalies, if accomplished, will likely provide valuable information not only about Martian photometry but for the design of future space camera systems and their calibration.

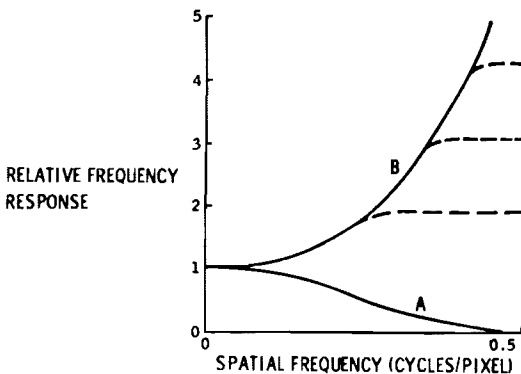
GEOMETRIC DISTORTION CORRECTIONS

In addition to projection distortions caused by oblique viewing, geometric distortions are introduced into television pictures by optical and electronic imaging aberrations. In the Mariner cameras both optical and electronic distortions exist, but the electronic are the more

severe. Electronic geometric distortions have the additional complication of varying in time because of internal electronic fluctuations and gross changes in the magnetic environment of the cameras, such as removal from the earth's magnetic field. The optical distortions are stable in time, within the resolution limits of the cameras, depending only on a stable mechanical mounting.

Calibration measurements were made to determine both the gross system distortions of combined optical and electronic origin, and the small time-varying electronic distortion changes. The composite distortion characteristics were measured before flight and were assumed to remain stable. The time-varying electronic distortions were measured for each frame in situ by means of an array of 63 black reseau points deposited directly on the vidicon target. The small changes in reseau positions from frame to frame describe the small changes to the over-all electronic distortion. A two-step geometric correction is thus made to the flight pictures. First, the reseau locations determined for each flight picture are corrected so as to coincide with the reseau locations in the composite distortion measurement. Then the composite correction is made to restore over-all geometric fidelity.

A calibration picture used to determine the



- A. TYPICAL VIDICON SYSTEM MTF
- B. IDEAL CORRECTION FILTER (NO NOISE LIMITATIONS)
- ARTIFICIAL ENHANCEMENT GAIN TRUNCATIONS TO OFFSET DEGRADING NOISE EFFECTS

Fig. 19. A plot of the preflight calibrated horizontal modulation transfer function for the Mariner 6 camera B and the theoretical reciprocal correction function. The truncated correction filter actually used applied a maximum gain of 1.5 and was based on observed camera-noise levels after noise removal.

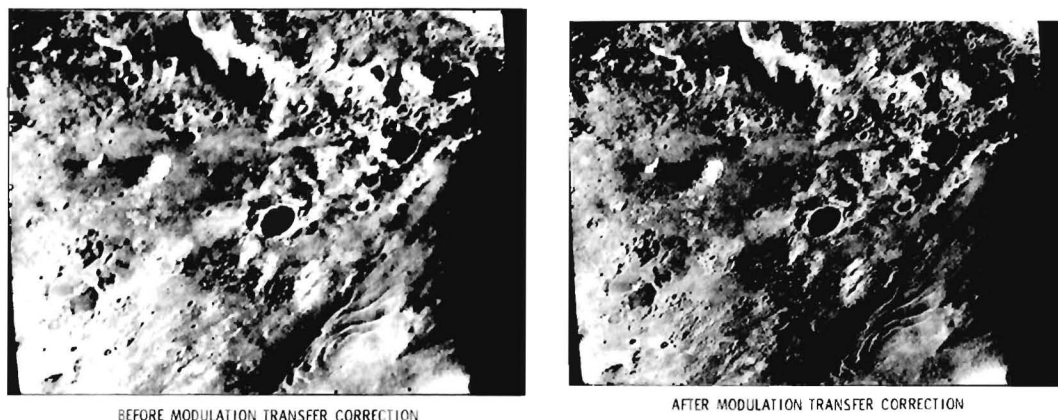


Fig. 20. A comparison of the results before and after applying the two-dimensional modulation transfer filter correction to Mariner 7 camera A picture 7N17. The version shown has not had the automatic-gain-control and cubing-amplifier corrections applied.

composite geometric parameters for a Mariner 6 camera is shown in Figure 17. The picture is the result of photographing an accurately scribed grid target with the camera. The orthogonality and regularity of the test grid were verified by theodolite measurements to be better than half the resolution limits of the camera system. Measurements of the positions of the grid intersections in the camera output and their vector displacements from the ideal distortionless locations provide a two-dimensional map of the picture-element position corrections. The correction is applied by a piecewise, linear interpolation of the grid-target-intersection data and determination of a position correction for every picture element in the frame. This single correction removes both optical and electronic distortions based on the electronic distortion characteristics at the time the calibration frame was taken. The geometrically corrected version of the calibration grid target is also shown in Figure 17.

The removal of the small frame-to-frame electronic distortions in the flight data is accomplished before this composite correction by correcting the reseau locations in the flight frames in such a way that the reseaux fall exactly upon those in the calibration picture from which the composite correction parameters were derived. This is accomplished in much the same way as the composite correction. The vector displacement of each reseau in a flight frame from the reference calibration location provides a net

that is a piecewise, linearly interpolated to correct the electronic distortion change for each picture element of the frame. The resultant pictures are then subjected to the composite correction. An example of the fully corrected flight frame 7N13 is shown in Figure 18. The cusp-like appearance of the upper left and lower right corners in the corrected frame indicate the severity of the electronic distortions in these areas. Displacements of up to 25 picture elements are common near the corners.

For the bulk of the far-encounter data, estimates of reseau locations had to be used for black space, since the black reseaux were not visible in those portions of the pictures not containing the planet. These estimates were generated by means of averaged positions for those reseaux based on subsequent data where the whole field was illuminated and the reseaux were visible. Because of the piecewise, linear interpolation algorithm used, errors in reseau locations far from the limb contribute negligibly to the geometric fidelity of the corrected planet data.

RESOLUTION ENHANCEMENT

The scale size of object-scene detail visible through a television camera is limited, in a perfect system, by diffraction effects in the optics. This, of course, ignores such effects as atmospheric turbulence. For most systems including the Mariner 1969 cameras, this limit is not realized as the camera sensor system itself imposes

resolution limitations that are dominant. The result is an apparent loss of contrast in small-scene detail (small relative to the resolution of the system) or, equivalently, a blurring of the transitions between adjacent intensities in the camera output.

If the camera system is linear or, as is the case for the Mariner 1969 mission, if the input scene is sufficiently low in contrast, the degradation in image resolution is described in terms of an amplitude-independent system point-spread function. If the point-spread function is furthermore independent of position in the image plane, such as for narrow-angle systems, then the camera output $O(x, y)$ can be written in terms of the object scene intensity distribution $I(x, y)$ and the system point-spread function $S(x, y)$ by a simple convolution relation

$$O(x, y) = \int du \int dv S(u, v) I(x + u, y + v)$$

This relation can be inverted by using Fourier transformations to express the desired input scene in terms of the camera output

$$I(x, y) = \int du \int dv F(u, v) O(x + u, y + v)$$

$F(x, y)$ is a correction filter related to the point-spread function through the relation

$$F(x, y) = \mathcal{F}^{-1} \left[\frac{1}{\mathcal{F}[S(x, y)]} \right]$$

where \mathcal{F} is the Fourier transform operator.

This sequence of equations has a discrete counterpart appropriate to digital computation. The additional condition of Nyquist sampling must be imposed in the discrete case for validity.

The correction filter function F is a function only of the uniform camera point-spread function and thus may be calibrated independently of the object scene. This is done for the Mariner 1969 experiment by measuring the modulation-transfer function (MTF) or the Fourier transform of the point-spread function rather than the point-spread function directly. The reason is that for vidicon systems, in order to produce a sufficient output point-spread amplitude to make reliable measurements for all spatial frequencies, the input must be so large as to drive the system into nonlinear response. The MTF is measured by exposing the camera to spatial

sine-wave transmittance targets of various frequencies and extracting the sine wave-amplitude degradation along the scan line and perpendicular to the scan-line directions [Danielson and Montgomery, 1971]. These curves are then used to model the two-dimensional MTF function by assuming the contours of equal response are ellipses. The phase component of the MTF is ignored, not so much because the omission is justified as because the measurement of phase properties has not been possible. The resulting MTF is then used to generate the correction filter.

The correction filter is theoretically the reciprocal of the MTF function. For typical systems however, the response at high spatial frequencies becomes quite low, so that gains in excess of ten at these frequencies are necessary. The addition of wideband noises within the system makes this theoretical correction undesirable. Since the scene spectral components decrease in amplitude at high frequencies and since the noise is essentially white, any filter correction degrades the gross signal-to-noise ratio of the resulting image. Thus some criterion for suppressing the large high-spatial-frequency gains is necessary on the basis of the competition between small-feature and edge-transition fidelity on the one hand and degraded signal-to-noise ratio on the other.

There are quantitative criteria for this trade-off such as the Wiener-Hopf filtering technique. For many purposes, however, these are unacceptable, since they are based on large-scale statistical measures of error and, in the small, produce less than optimum results.

For many purposes a simple trial and error solution to the problem is adequate. In Figure 19 a typical MTF curve for the Mariner cameras is shown and labelled 'A.' The theoretical correction filter based on this MTF is shown as curve 'B.' By introducing an artificial truncation to the theoretical curve, as shown in the dashed curves, the emphasis of high-spatial-frequency noise amplification can be controlled. A filter or series of filters consistent with the camera signal-to-noise properties, the typical scene-spatial-frequency composition, and experiment measurement goals can be derived.

For Mariner 1969, primarily because of the severe noise problems, the modulation-transfer correction had to be truncated with a high-

spatial-frequency gain of 1.5. Even so, a significant sharpening of surface detail was produced, as is seen in the comparison of the Mariner 7 photographs of Figure 20.

These corrections were applied as a convolution filter with the kernel generated from the reciprocal MTF function rather than as a direct-frequency space filter. The reason is strictly one of economy. The convolution kernel matrix for these corrections needs to be only on the order of 15 picture elements square, and increased calculation speed is realized by matrix convolution rather than transformation. This trade-off is in contrast to that of the previously discussed periodic noise filtering. In order to obtain sufficiently narrow frequency space bandpass characteristics, the convolution kernel would be prohibitively large, thereby making direct-transform space filtering the more economical approach.

SUMMARY

The extended coverage and high surface-feature discriminability goals of the Mariner Mars 1969 television experiment resulted in the design of a highly complex video system. This design included as a prerequisite to quantitative image interpretation the extensive restorative and corrective processing of the Mars photographs. Because of the nonlinear distortions inherent in vidicon and in fact most television sensors, and because of the complex nonlinear encoding scheme evolved, the flexibility of the digital computer was required to produce the desired images portraying Mars as it actually appeared. The successful accomplishment of

this most difficult task has produced a set of data significantly extending man's knowledge of Mars and has demonstrated the power of digital techniques as an adjunct to the interpretation of video data.

Acknowledgments. The task of calibrating and processing the Mariner Mars 1969 photographs was very large and included contributions from many people at the Jet Propulsion Laboratory in addition to the authors. The contributions of the following are hereby gratefully acknowledged: F. C. Billingsley, D. Brown, S. A. Collins, G. E. Danielson, E. F. Dobies, A. R. Gillespie, E. T. Johnson, D. Mathews, J. M. Soha, K. R. Taylor, G. M. Tetsuka, T. E. Thorpe, and V. W. Tuk. In addition the authors gratefully acknowledge the cooperation, patience, and advice of the Mariner Mars 1969 Television Experiment Team members and in particular the help of Professor R. B. Leighton.

This paper presents the results of one phase of research conducted at the Jet Propulsion Laboratory, California Institute of Technology, under contract NAS 7-100, sponsored by the National Aeronautics and Space Administration.

REFERENCES

- Danielson, G. E., and D. R. Montgomery, Calibration of the Mariner Mars 1969 television cameras, *J. Geophys. Res.*, 76, this issue, 1971.
- Dunne, J. A., W. D. Stromberg, R. M. Ruiz, S. A. Collins, and T. E. Thorpe, Maximum discriminability versions of the near-encounter Mariner pictures, *J. Geophys. Res.*, 76, this issue, 1971.
- Leighton, R. B., and B. C. Murray, One year's processing and interpretation—an overview, *J. Geophys. Res.*, 76, this issue, 1971.
- Nathan, R., Digital video-data handling, *Jet Propul. Lab. TR 32-877*, 1966.

(Received August 10, 1970;
revised September 15, 1970.)